

The CHESS chemical Herschel surveys of star forming regions: Peering into the protostellar shock L1157-B1

I. Shock chemical complexity^{*}

Codella C.¹, Lefloch B.², Ceccarelli C.², Cernicharo J.³, Caux E.⁴, Lorenzani A.¹, Viti S.^{5,6}, Hily-Blant P.², Parise B.⁷, Maret S.², Nisini B.⁸, Caselli P.^{9,1}, Cabrit S.¹⁰, Pagani L.¹⁰, Benedettini M.⁶, Boogert A.¹¹, Gueth F.¹², Melnick G.¹³, Neufeld D.¹⁴, Pacheco S.², Salez M.¹⁰, Schuster K.¹², Bacmann A.^{2,15}, Baudry A.¹⁵, Bell T.¹⁶, Bergin E.A.¹⁷, Blake G.¹⁶, Bottinelli S.⁴, Castets A.², Comito C.⁷, Coutens A.⁴, Crimier N.^{2,3}, Dominik C.^{18,19}, Demyk K.⁴, Encrenaz P.¹⁰, Falgarone E.¹⁰, Fuente A.²⁰, Gerin M.¹⁰, Goldsmith P.²¹, Helmich F.²², Hennebelle P.¹⁰, Henning Th.²³, Herbst E.²⁴, Jacq T.¹⁵, Kahane C.², Kama M.¹⁸, Klotz A.², Langer W.²¹, Lis D.¹⁶, Lord S.¹⁶, Pearson J.²¹, Phillips T.¹⁶, Saraceno P.⁶, Schilke P.^{7,25}, Tielens X.²⁶, van der Tak F.²², van der Wiel M.^{27,22}, Vastel C.⁴, Wakelam V.¹⁵, Walters A.⁴, Wyrowski F.⁷, Yorke H.²¹, Borys C.¹⁶, Delorme Y.¹⁰, Kramer C.²⁸, Larsson B.²⁹, Mehdi I.²¹, Ossenkopf V.²⁵, and Stutzki J.²⁵

(Affiliations can be found after the references)

Received date; accepted date

ABSTRACT

We present the first results of the unbiased survey of the L1157-B1 bow shock, obtained with HIFI in the framework of the key program Chemical *Herschel* surveys of star forming regions (CHESS). The L1157 outflow is driven by a low-mass Class 0 protostar and is considered the prototype of the so-called chemically active outflows. The bright blue-shifted bow shock B1 is the ideal laboratory for studying the link between the hot (~ 1000 – 2000 K) component traced by H_2 IR-emission and the cold (~ 10 – 20 K) swept-up material. The main aim is to trace the warm gas chemically enriched by the passage of a shock and to infer the excitation conditions in L1157-B1. A total of 27 lines are identified in the 555–636 GHz region, down to an average 3σ level of 30 mK. The emission is dominated by $\text{CO}(5-4)$ and $\text{H}_2\text{O}(1_{10}-1_{01})$ transitions, as discussed by Lefloch et al. in this volume. Here we report on the identification of lines from NH_3 , H_2CO , CH_3OH , CS , HCN , and HCO^+ . The comparison between the profiles produced by molecules released from dust mantles (NH_3 , H_2CO , CH_3OH) and that of H_2O is consistent with a scenario in which water is also formed in the gas-phase in high-temperature regions where sputtering or grain-grain collisions are not efficient. The high excitation range of the observed tracers allows us to infer, for the first time for these species, the existence of a warm (≥ 200 K) gas component coexisting in the B1 bow structure with the cold and hot gas detected from ground.

Key words. ISM: individual objects: L1157 — ISM: molecules — stars: formation

1. Introduction

A newborn protostar generates a fast and well collimated jet, possibly surrounded by a wider angle wind. In turn, the ejected material drives (bow-)shocks travelling through the surrounding high-density medium and traced by H_2 ro-vibrational lines at excitation temperatures of around 2000 K. As a consequence, slower and cold (10–20 K) molecular outflows are formed by swept-up material, usually traced by CO. Shocks heat the gas and trigger several processes such as endothermic chemical reactions and ice grain mantle sublimation or sputtering. Several molecular species undergo significant enhancements in their abundances (see e.g., van Dishoeck & Blake 1998), as observed by observations at millimeter wavelengths towards a number of outflows (Garay et al. 1998; Bachiller & Pérez Gutiérrez 1997, BP97 hereafter; Jørgensen et al. 2007). The link between the gas components at ~ 10 K and the hot 2000 K shocked component is crucial to understanding how the protostellar wind transfers momentum and energy back to the ambient medium. In this context, the understanding of the chemical composition of a typical

molecular bow-shock is essential because it represents a very powerful diagnostic tool for probing its physical conditions.

The L1157 outflow, located at a distance estimated to be between 250 pc (Looney et al. 2007) and 440 pc (Viotti 1969) may be regarded as the ideal laboratory for observing the effects of shocks on the gas chemistry, being the archetype of the so-called chemically rich outflows (Bachiller et al. 2001). The low-luminosity (4 – $11 L_\odot$) Class 0 protostar IRAS20386+6751 drives a precessing powerful molecular outflow associated with several bow shocks seen in CO (Gueth et al. 1996) and in IR H_2 images (Davis & Eislöffel 1995; Neufeld et al. 2009). In particular, the brightest blue-shifted bow-shock, called B1 (Fig. 1), has been extensively mapped with the PdB and VLA interferometers at mm- and cm-observations revealing a rich and clumpy structure, the clumps being located at the wall of the cavity with an arch-shape (Tafalla & Bachiller 1995; Gueth et al. 1998; Benedettini et al. 2007, hereafter BVC07; Codella et al. 2009). L1157-B1 is well traced by molecules thought to be released by dust mantles such as H_2CO , CH_3OH , and NH_3 as well as typical tracers of high-speed shocks such as SiO (e.g., Gusdorf et al. 2008). Temperatures $\simeq 60$ – 200 K (from NH_3 , CH_3CN , and SiO) as well as around 1000 K (from H_2) have been derived (Tafalla & Bachiller 1995; Codella et al. 2009; Nisini et al. 2007, in prep.).

^{*} *Herschel* is an ESA space observatory with science instruments provided by European-led principal Investigator consortia and with important participation from NASA

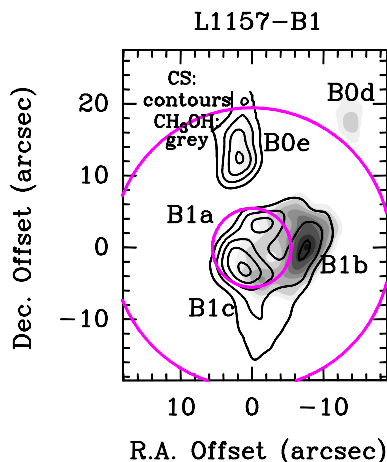


Fig. 1. The B1 clump. PdBI emission of $\text{CH}_3\text{OH}(2_1-1_1)\text{A}^-$ (grey) on the $\text{CS}(2-1)$ one (contours), from BVC07. The maps are centred on the coordinates used for the present HIFI observations $\alpha_{\text{J2000}} = 20^{\text{h}} 39^{\text{m}} 10^{\text{s}}.2$, $\delta_{\text{J2000}} = +68^\circ 01' 10''.5$, i.e. at $\Delta\alpha = +25''.6$ and $\Delta\delta = -63''.5$ from the driving protostar. The labels indicate the main B1 clumps detected in different tracers. Circles are for the HPBW of the HIFI data presented here ($39''$) and of Band 7 ($11''$), i.e., at the highest frequencies of the CHESSE surveys.

However, a detailed study of the excitation conditions of the B1 structure has yet to be completed because of the limited range of excitation covered by the observations performed so far at cm- and mm-wavelengths. Observations of sub-mm lines with high excitation (≥ 50 – 100 K above the ground state) are thus required.

As part of the *Herschel* Key Program CHESSE¹ (Chemical *Herschel* Surveys of Star forming regions), L1157-B1 is currently being investigated with an unbiased spectral survey using the HIFI instrument (de Graauw et al. 2010). In this Letter, we report the first results based on HIFI observations in the 555–636 GHz spectral window, confirming the chemical richness and revealing different molecular components at different excitation conditions coexisting in the B1 bow structure.

2. Observations

The observations were performed on 2009, August 1, during the Performance Verification phase of the HIFI heterodyne instrument (de Graauw et al. 2010) on board of the *Herschel* Space Observatory (Pilbratt et al. 2010). The band called 1b (555.4–636.2 GHz) was covered in double-sideband (DSB) with a total integration time of 140 minutes. The Wide Band Spectrometer was used with a frequency resolution of 1 MHz. The typical HPBW is $39''$. The data were processed with the ESA-supported package HIPE² (*Herschel* Interactive Processing Environment) for baseline subtraction and sideband deconvolution and then analysed with the GILDAS³ software. All the spectra (here in units of antenna T_{a}) were smoothed to a velocity resolution of 1 km s^{-1} , except those showing the weakest emission, which were smoothed to lower spectral resolutions (up to 4 km s^{-1}). At a velocity resolution of 1 km s^{-1} , the rms noise is 6–13 mK

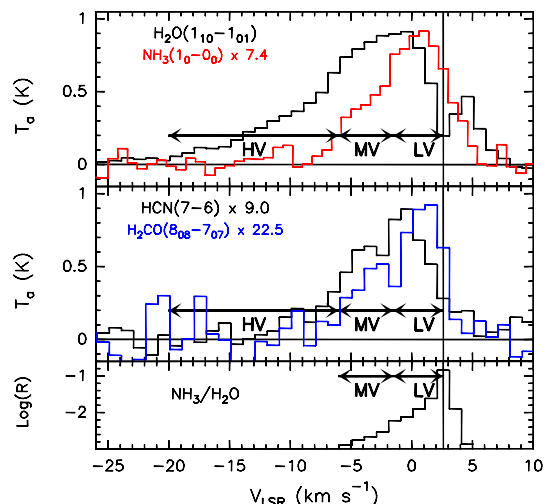


Fig. 3. *Top and Middle panel:* Comparison between the profiles of $\text{NH}_3(1_0-0_0)$, multiplied by a factor 7.4, $\text{H}_2\text{CO}(8_{17}-7_{16})$, multiplied by a factor 22.5, $\text{HCN}(7-6)$, multiplied by a factor 9.0, and $\text{H}_2\text{O}(1_{10}-1_{01})$, the latter from Lefloch et al. (2010). The vertical solid line indicates the ambient LSR velocity ($+2.6 \text{ km s}^{-1}$). The velocity ranges arbitrarily defined as HV ($-20, -6 \text{ km s}^{-1}$; traced by H_2O), MV ($-6, -1.5 \text{ km s}^{-1}$; outlined by the HCN and H_2CO secondary peak), and LV ($-1.5, +2.6 \text{ km s}^{-1}$; the rest of the blue wing) are drawn (see text). *Bottom panel:* Intensity $\text{NH}_3/\text{H}_2\text{O}$ line ratio as a function of velocity.

(T_{a} scale), depending on the line frequency. The main-beam efficiency (η_{mb}) has not yet been reliably determined. When needed, we adopted an average η_{mb} of 0.72.

3. Different tracers at different velocities

A total of 27 emission lines were detected, with a wide range of upper level energies, from a few tens to a few hundreds of Kelvin. Table 1 lists the spectroscopic and observational parameters of all the transitions. For the first time, high excitation (up to ≈ 200 K) emission lines related to species whose abundance is largely enhanced in shocked regions were detected. The $\text{CO}(5-4)$ and $\text{H}_2\text{O}(1_{10}-1_{01})$ lines are analysed in Lefloch et al. (2010). Figure 2 presents representative examples of line profiles observed towards L1157-B1. All the spectra contain lines with blue-shifted wings peaking near 0 km s^{-1} , which have a terminal velocity equal to $\sim -8, -6 \text{ km s}^{-1}$. Previous PdBI observations showed that L1157-B1 is associated with very high velocities (HVs) of as low as $\approx -20 \text{ km s}^{-1}$ ($v_{\text{LSR}} = +2.6 \text{ km s}^{-1}$, BP97). We cannot exclude the lack of detected emission in the HV regime in the present HIFI spectra being caused by their relatively low signal-to-noise (S/N) ratio. The PdBI images indicate that the brightness of the emission lines in the HV regime is indeed weaker than the emission at low velocities by a factor of 5–10. The spectra in Fig. 2 clearly show that this weak emission would lie below the noise. On the other hand, the HV gas is detected in the very bright lines of CO and H_2O (Lefloch et al. 2010). We note that the HV emission is mostly confined to within the eastern B1a clump (Fig. 1), within an emitting region of size $\leq 10''$ (Gueth et al. 1998; BVC07), whereas low velocity lines originate in both the bow-structure and the walls of the outflow cavity (e.g., the B0e and B0d in Fig. 1), of typical size $15''$ – $18''$. Therefore, the forthcoming HIFI-CHESSE observations at higher frequencies and higher spatial resolution (see

¹ <http://www-laog.obs.ujf-grenoble.fr/heberges/chess/>

² HIPE is a joint development by the *Herschel* Science Ground Segment Consortium, consisting of ESA, the NASA *Herschel* Science Center, and the HIFI, PACS and SPIRE consortia.

³ <http://www.iram.fr/IRAMFR/GILDAS>

Table 1. List of molecular species and transitions observed with HIFI (Band 1b): CO and H₂O emission is discussed in Lefloch et al. (2010). Peak velocity and intensity (in T_a scale), integrated intensity (F_{int}), as well as the terminal velocities of the line emission (V_{min} and V_{max}) are reported.

Transition	ν_0^a (MHz)	E_u^a (K)	T_{peak} (mK)	rms (mK)	V_{peak} (km s ⁻¹)	V_{min} (km s ⁻¹)	V_{max} (km s ⁻¹)	F_{int} (K km s ⁻¹)
o-H ₂ O(1 ₁₀ -1 ₀₁)	556936.002	27	910(17)	17	-0.37(1.00)	-25.4	+7.6	11.68(0.10)
CH ₃ OH E (11 _{2,9} - 10 _{1,9})	558344.500	168	47(10)	10	+0.60(1.00)	-2.9	+2.7	0.16(0.02)
o-H ₂ CO(8 ₁₈ -7 ₁₇)	561899.318	118	92(4) ^b	8	+0.38(0.14) ^b	-4.5	+3.6	0.49(0.03) ^b
CH ₃ OH E (3 _{2,2} - 2 _{1,2})	568566.054	32	42(8)	8	+0.60(1.00)	-2.6	+2.7	0.31(0.02)
o-NH ₃ (1 ₀ -0 ₀)	572498.068	28	122(7)	7	+1.03(0.80)	-6.9	+5.0	0.89(0.03)
CO(5-4)	576267.931	83	883(10)	10	+1.60(1.00)	-36.5	+6.0	49.30(0.07)
p-H ₂ CO(8 ₀₈ -7 ₀₇)	576708.315	125	41(7)	7	+1.80(1.00)	-5.4	+2.7	0.22(0.02)
CH ₃ OH A ⁻ (2 _{2,1} - 1 _{1,0})	579084.700	45	53(8)	8	+0.60(1.00)	-6.0	+3.7	0.29(0.03)
CH ₃ OH E (12 _{1,12} - 11 _{1,11})	579151.003	178	44(8)	8	-0.30(1.00)	-4.0	+4.0	0.25(0.02)
CH ₃ OH A ⁺ (12 _{0,12} - 11 _{0,11})	579459.639	181	48(7)	7	+0.90(1.00)	-3.9	+4.9	0.27(0.02)
CH ₃ OH A ⁺ (2 _{2,0} - 1 _{1,1})	579921.342	45	42(7)	7	-0.60(1.00)	-3.3	+2.6	0.21(0.02)
CH ₃ OH E (12 _{2,10} - 11 _{2,9})	580902.721	195	11(4)	4	-3.00(3.00)	-3.9	+2.5	0.09(0.02)
CH ₃ OH A ⁺ (6 _{1,6} - 5 _{0,5})	584449.896	63	88(9)	9	-0.30(1.00)	-6.0	+2.9	0.58(0.03)
CS(12-11)	587616.240	183	23(2) ^b	5	-0.61(0.57) ^b	-7.3	+6.5	0.19(0.03) ^b
CH ₃ OH A ⁺ (7 _{3,5} - 6 _{2,4})	590277.688	115	42(9)	9	+0.60(1.00)	-1.0	+3.0	0.16(0.02)
CH ₃ OH A ⁻ (7 _{3,4} - 6 _{2,5})	590440.291	115	40(9)	9	-0.60(1.00)	-2.6	+0.8	0.10(0.02)
CH ₃ OH E (9 _{0,9} - 8 _{1,8})	590790.957	110	40(10)	10	+0.60(1.00)	-4.7	+4.3	0.28(0.03)
o-H ₂ CO(8 ₁₇ -7 ₁₆)	600374.604	126	29(7) ^b	9	-0.14(0.57) ^b	-3.0	+1.8	0.19(0.04) ^b
CH ₃ OH E (4 _{2,3} - 3 _{1,3})	616979.984	41	47(6)	6	+0.90(1.00)	-4.5	+2.6	0.26(0.02)
HCN(7-6)	620304.095	119	94(7)	7	-0.60(1.00)	-7.6	+3.2	0.68(0.03)
HCO ⁺ (7-6)	624208.180	119	30(3) ^b	8	+0.53(0.47) ^b	-3.6	+4.5	0.11(0.03) ^b
CH ₃ OH A ⁻ (3 _{2,2} - 2 _{1,1})	626626.302	52	18(5)	5	-1.20(4.00)	-2.5	+6.3	0.18(0.07)
CH ₃ OH E (13 _{1,13} - 12 _{1,12})	627170.503	209	33(7)	7	-0.30(1.00)	-3.2	+2.5	0.15(0.02)
CH ₃ OH A ⁺ (13 _{0,13} - 12 _{0,12})	627558.440	211	41(9)	9	+0.60(1.00)	-3.6	+2.5	0.19(0.02)
CH ₃ OH A ⁺ (3 _{1,2} - 2 _{1,2})	629140.493	52	52(9)	9	+0.60(1.00)	-3.5	+3.7	0.24(0.03)
CH ₃ OH A ⁺ (7 _{1,7} - 6 _{0,6})	629921.337	79	70(13)	13	+1.50(1.00)	-3.9	+3.7	0.37(0.04)
o-H ₂ CO(9 ₁₉ -8 ₁₈)	631702.813	149	66(4) ^b	9	+0.45(0.17) ^b	-1.5	+2.6	0.22(0.02) ^b

^a Frequencies and spectroscopic parameters have been extracted from the Jet Propulsion Laboratory molecular database (Pickett et al. 1998) for all the transition except those of CH₃OH, which have been extracted from the Cologne Database for Molecular Spectroscopy (Müller et al. 2005). Upper level energies refer to the ground state of each symmetry. ^b Gaussian fit.

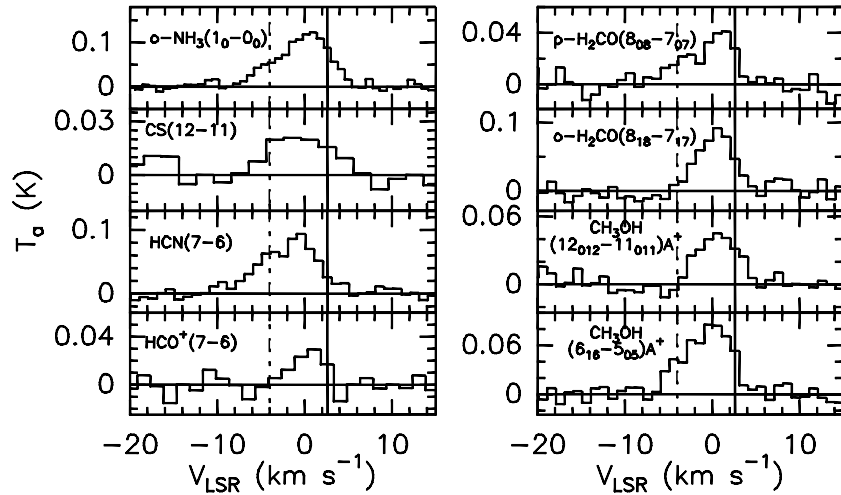


Fig. 2. Molecular line profiles observed towards L1157-B1: species and transitions are reported in the panels. The vertical solid line indicates the ambient LSR velocity (+2.6 km s⁻¹ from C¹⁸O emission; BP97), while the dashed one is for the secondary peak at -4.0 km s⁻¹.

the dashed circle in Fig. 1) should allow us to study the HV wings in species other than CO and H₂O.

The uniqueness of HIFI lies in its high spectral profile resolution for many high excitation transitions of a large number of molecular species. The analysis of the present HIFI spectra reveals a secondary peak occurring between -3.0 and -4.0 km s⁻¹

(here defined medium velocity, MV) and well outlined by e.g., HCN(7-6). The MV peak is also visible in NH₃(1₀-0₀) and in some lines of CH₃OH and H₂CO (see Fig. 3), but its occurrence does not show any clear trend with the choice of tracer of line excitation. No single-dish spectra had previously detected this spectral feature (BP97; Bachiller et al. 2001). An inspection of

the spectra observed at PdBI shows that the MV secondary peak is observed in a couple of lines of the $\text{CH}_3\text{OH}(2_K-1_K)$ series (see Fig. 3 of BVC07) and only towards the western B1b clump (size $\sim 5''$). This finding implies that there is a velocity component originating mainly in the western side of B1, while the HV gas is emitted from the eastern one (see above).

Figure 3 compares the profiles of the $\text{NH}_3(1_0-0_0)$ and $\text{H}_2\text{CO}(8_{17}-7_{16})$ lines with the $\text{H}_2\text{O}(1_{10}-1_{01})$ profile, where the S/N allows such an analysis (MV and LV ranges). By assuming that the emission in the MV range is optically thin (including the H_2O line) and originates in the same region, we obtained from the comparison of their profiles a straightforward estimate of the relative abundance ratios of the gas at different velocities. As a notable example, the $\text{NH}_3/\text{H}_2\text{O}$ intensity ratio decreases by a factor ~ 5 moving towards higher velocities (Fig. 3), implying that a similar decrease in the abundance ratios occurs. This may reflect different pre-shock ice compositions in the gas emitting the MV emission. Alternatively, this behavior is consistent with NH_3 being released by grain mantles, but water both being released by grain mantles and, in addition, copiously forming in the warm shocked gas from endothermic reactions, which convert all gaseous atomic oxygen into water (Kaufman & Neufeld 1997; Jiménez-Serra et al. 2008, and references therein). The water abundance may be enhanced with respect to ammonia in the fast and warm (≥ 220 K) gas, which might explain why the H_2O wings are larger than those of NH_3 , CH_3OH , and H_2CO , all species being directly evaporated from dust grain mantles.

4. Physical properties along the B1 bow shock

We detected several lines from CH_3OH (17 lines with upper level energies up to 211 K). We can derive a first estimate of the emitting gas temperature by means of the standard analysis of the rotational diagram. We show the case of methanol (A- and E-forms) in Fig. 4. The derived rotational temperature (T_{rot}) is 106 K (with an uncertainty of ~ 20 K), which represents a lower limit to the kinetic temperature (T_{kin}). In the same figure, we report the methanol lines (2_K-1_K) observed with PdBI and whose intensity is integrated in the HIFI 39'' beam. The T_{rot} derived from the ground-based data (based only on lines with $E_u \leq 50$ K; BVC07) is definitely lower, ~ 12 K, in perfect agreement with that found with the 30-m spectra in the same excitation range by Bachiller et al. (1995). As discussed by Goldsmith & Langer (1999), this behavior may be caused by either two components at different temperatures or both non-LTE effects and line opacity. These two possibilities cannot be distinguished based only on the rotational diagram. However, given that a range of T_{kin} and n_{H_2} is naturally expected in a shock, if we were to assume that two gas components provide an explanation, they would not only have different temperatures but also a different column densities. Taking the filling factor $\text{ff} = 0.13$, derived by the CH_3OH maps obtained at the PdBI, the low temperature component column density is $8 \times 10^{14} \text{ cm}^{-2}$ (in agreement with Bachiller et al. 1995), whereas the high temperature component has a column density of around 10^{14} cm^{-2} . We note that the rotation diagrams obtained for the MV and LV CH_3OH emission separately do not allow us to infer any clear difference.

It is possible to more tightly constrain the emitting gas temperature and n_{H_2} density for the species where the collisional rate coefficients are known, by performing of a non-LTE analysis. To this end, we used the non-LTE excitation code RADEX with an escape probability formalism for the radiative transfer (Van der Tak et al. 2007) coupled with the LAMDA database (Schöier et al. 2005). Methanol is the species detected in the largest num-

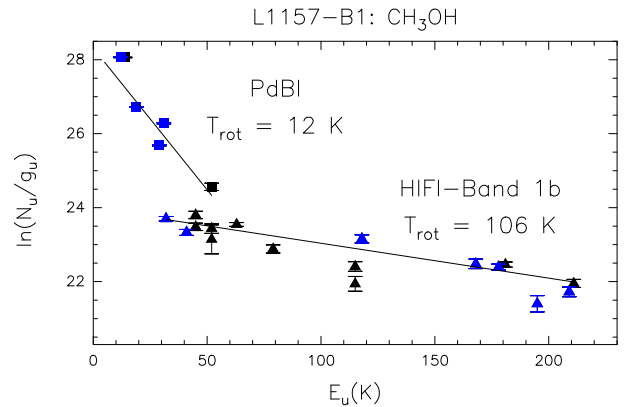


Fig. 4. Rotation diagrams for the CH_3OH transitions measured with HIFI (triangles) and from ground (PdBI; squares). Black and blue points are for A- and E-form, respectively. The parameters N_u , g_u , and E_u are, respectively, the column density, the degeneracy and the energy (with respect to the ground state of each symmetry) of the upper level. The derived values of the rotational temperature are reported: (i) 106 K, for the HIFI lines covering the $E_u = 32$ -211 K excitation range and (ii) 12 K (as Bachiller et al. 1995), for the PdBI lines, at lower excitation.

ber of lines. The full non-LTE study will be reported in a forthcoming paper. Here we analysed only the E-form, for which the collisional rate coefficients are available (Pottage et al. 2004). The major result of this analysis is that for a range of densities of 10^3 - 10^7 cm^{-3} , the gas temperature exceeds 200 K. A similar result is obtained by considering H_2CO emission.

Finally, by combining the HIFI CS(12-11) line with CS(2-1) and (3-2) lines observed with ground-based telescopes, we also derive a kinetic temperature that is definitely above 300 K for the outflowing gas. In this case, caution should be taken since we are able to trace different gas components, as suggested by CH_3OH , the gas at higher excitation being traced by CS(12-11). If we analyse only the (2-1)/(3-2) intensity ratio, the non-LTE approach does not allow us to constrain the temperature in this way, but we are able to infer n_{H_2} of around $4 \times 10^4 \text{ cm}^{-3}$. Interestingly, when we check for a possible dependence of n_{H_2} on velocity, the LV range is found to be indicative of a denser medium ($\sim 10^5 \text{ cm}^{-3}$) by an order of magnitude with respect to the MV gas.

5. Conclusions

We have presented the HIFI unbiased spectral survey in the 555-636 GHz band towards the bright bow-shock B1 of the L1157 protostellar outflow. For the first time, we have detected high-excitation (up to ≈ 200 K) emission lines of species whose abundance is largely enhanced in shocked regions (e.g., H_2O , NH_3 , H_2CO , CH_3OH). This has allowed us to trace with these species the existence of a high excitation component with $T_{\text{kin}} \geq 200$ -300 K. Temperature components from ~ 300 K to ~ 1400 K have been inferred from the analysis of the H_2 pure rotational lines (Nisini et al., in prep.). Therefore the present observations provide a link between the gas at $T_{\text{kin}} 60$ -200 K previously observed from the ground and the warmer gas probed by the H_2 lines. We plan to perform additional HIFI observations in the THz region towards L1157-B1 to observe more species and transitions, thus to be able to derive reliable abundances and study of the different gas components associated with the bow structure.

Acknowledgements. HIFI has been designed and built by a consortium of institutes and university departments from across Europe, Canada and the United States under the leadership of SRON Netherlands Institute for Space Research, Groningen, The Netherlands and with major contributions from Germany, France and the US. Consortium members are: Canada: CSA, UWaterloo; France: CESR, LAB, LERMA, IRAM; Germany: KOSMA, MPIfR, MPS; Ireland, NUI Maynooth; Italy: ASI, IFSI-INAF, Osservatorio Astrofisico di Arcetri-INAF; Netherlands: SRON, TUD; Poland: CAMK, CBK; Spain: Observatorio Astronómico Nacional (IGN), Centro de Astrobiología (CSIC-INTA). Sweden: Chalmers University of Technology - MC2, RSS & GARD; Onsala Space Observatory; Swedish National Space Board, Stockholm University - Stockholm Observatory; Switzerland: ETH Zurich, FHNW; USA: Caltech, JPL, NHSC. We thank many funding agencies for financial support.

References

- Bachiller R., & Peréz Gutiérrez M. 1999, *ApJ*, 487, L93 (BP97)
- Bachiller R., Liechti S., Walmsley C.M., & Colomer F. 1995, *A&A*, 295, L51
- Bachiller R., Peréz Gutiérrez M., Kumar M.S.N., & Tafalla M. 2001, *A&A* 372, 899
- Benedettini M., Viti S., Codella C., et al. 2007, *MNRAS*, 381, 1127 (BVC07)
- Codella C., Benedettini M., Beltrán M.T., et al. 2009, *A&A*, 507, L25
- Davis C.J., & Eisloffel J. 1995, *A&A* 300, 851
- de Graauw Th., et al. 2010, this volume
- Garay G., Köhnenkamp I., Bourke T.L., Rodríguez L.F., & Lehtinen K.K. 1998, *ApJ*, 509, 768
- Goldsmith P.F. & Langer W.D. 1999, *ApJ*, 517, 209
- Gueth F., Guilloteau S., & Bachiller R. 1996, *A&A* 307, 891
- Gueth F., Guilloteau S., & Bachiller R. 1998, *A&A*, 333, 287
- Gusdorf A., Pineau Des Forêts G., Cabrit S., & Flower D.R. 2008, *A&A* 490, 695
- Jiménez-Serra I., Caselli P., Martín-Pintado J., & Hartquist T.W. 2008, *A&A* 482, 549
- Jørgensen J.K., Bourke T.L., & Myers P.C. 2007, *ApJ*, 659, 479
- Lefloch B., Cabrit S., Codella C., et al. 2010, this volume
- Looney L.W., Tobin J.J., & Kwon W. 2007, *ApJ*, 670, L131
- Müller H.S.P., Schöier F.L., Stutzki J., & Winnewisser G. 2005, *J.Mol.Struct.*, 742, 215
- Neufeld D.A., Nisini B., Giannini T., et al. 2009, *ApJ*, 706, N09
- Nisini B., Codella C., Giannini T., et al. 2007, *A&A*, 462, 163
- Pickett H.M., Poynter R.L., Cohen E.A., Delitsky M.L., Pearson J.C., and Müller H.S.P. 1998, *J. Quant. Spectrosc. & Rad. Transfer*, 60, 883
- Pilbratt G., et al. 2010, this volume
- Pottage J.T., Flower D.R., & Davis S.L. 2004, *MNRAS*, 352, 39
- Schöier F.L., van der Tak F.F.S., van Dishoeck E.F., & Black J.H. 2005, *A&A*, 432, 369
- Tafalla M., & Bachiller R. 1995, *ApJ* 443, L37
- Viotti N.R. 1969, *Mem. Soc. Astron. Ital.*, 40, 75
- van Dishoeck E.F., & Blake G.A. 1998, *ARA&A*, 36, 317
- Van der Tak F.F.S., Black J.H., Schöier F.L., Jansen D.J., & van Dishoeck, E.F. 2007, *A&A*, 468, 627
- ¹⁶ California Institute of Technology, Pasadena CA, USA
- ¹⁷ University of Michigan, Ann Arbor, MI 48109, USA
- ¹⁸ Astronomical Institute 'Anton Pannekoek', University of Amsterdam, Amsterdam, The Netherlands
- ¹⁹ Department of Astrophysics/IMAPP, Radboud University Nijmegen, Nijmegen, The Netherlands
- ²⁰ IGN Observatorio Astronómico Nacional, Alcalá de Henares, Spain
- ²¹ Jet Propulsion Laboratory, Caltech, Pasadena, CA 91109, USA
- ²² SRON, Institute for Space Research, Groningen, The Netherlands
- ²³ Max-Planck-Institut für Astronomie, Heidelberg, Germany
- ²⁴ Ohio State University, Columbus OH, USA
- ²⁵ Physikalisches Institut, Universität zu Köln, Köln, Germany
- ²⁶ Leiden Observatory, Leiden University, Leiden, The Netherlands
- ²⁷ Kapteyn Astronomical Institute, Groningen, The Netherlands
- ²⁸ Institut de RadioAstronomie Millimétrique, Granada, Spain
- ²⁹ Department of Astronomy, Stockholm University, Stockholm, Sweden
- ¹ INAF, Osservatorio Astrofisico di Arcetri, Firenze, Italy: e-mail: codella@arcetri.astro.it
- ² Laboratoire d'Astrophysique de Grenoble, UMR 5571-CNRS, Université Joseph Fourier, Grenoble, France
- ³ Centro de Astrobiología, CSIC-INTA, Madrid, Spain
- ⁴ CESR, Université Toulouse 3 and CNRS, Toulouse, France
- ⁵ Department of Physics and Astronomy, University College London, London, UK
- ⁶ INAF, Istituto di Fisica dello Spazio Interplanetario, Roma, Italy
- ⁷ Max-Planck-Institut für Radioastronomie, Bonn, Germany
- ⁸ INAF, Osservatorio Astronomico di Roma, Monte Porzio Catone, Italy
- ⁹ School of Physics and Astronomy, University of Leeds, Leeds, UK
- ¹⁰ Observatoire de Paris-Meudon, LERMA UMR CNRS 8112. Meudon, France
- ¹¹ Infrared Processing and Analysis Center, Caltech, Pasadena, USA
- ¹² Institut de RadioAstronomie Millimétrique, Grenoble, France
- ¹³ Center for Astrophysics, Cambridge MA, USA
- ¹⁴ Johns Hopkins University, Baltimore MD, USA
- ¹⁵ CNRS/INSU, Laboratoire d'Astrophysique de Bordeaux, Floirac, France